Chemical Engineering Journal 322 (2017) 445–453

Contents lists available at ScienceDirect

Chemical Engineering Journal

journal homepage: www.elsevier.com/locate/cej

Photoresponsive polyelectrolyte/mesoporous silica hybrid materials with remote-controllable ionic transportation

Wei Li [a,1], Tairong Kuang [b,*,1], Xiaoping Jiang [a], Jintao Yang [a], Ping Fan [a], Zhengping Zhao [a], Zhengdong Fei [a], Mingqiang Zhong [a], Lingqian Chang [d,*], Feng Chen [a,c,*]

[a] College of Materials Science and Engineering, Zhejiang University of Technology, Hangzhou 310014, China
[b] National Engineering Research Center of Novel Equipment for Polymer Processing, The Key Laboratory of Polymer Processing Engineering of Ministry of Education, South China University of Technology, Guangzhou 510640, China
[c] NSEC Center for Affordable Nanoengineering of Polymeric Biomedical Devices, The Ohio State University, Columbus, OH 43210, USA
[d] Department of Mechanical Engineering, Northwestern University, Evanston, IL 60208, USA

HIGHLIGHTS

- A azobenzene copolymer grafted from the mesoporous silica was prepared by RAFT.
- The copolymer could be used as a light-triggered and controllable ions transport system.
- The ion conductivity could be controlled in response to environmental stimuli.
- A prototype of light-triggered hybrid sensor was successfully fabricated.
- The sensor presented "gate on/off" sate under UV light irradiation.

ARTICLE INFO

Article history:
Received 13 January 2017
Received in revised form 10 April 2017
Accepted 11 April 2017
Available online 12 April 2017

Keywords:
Polyelectrolyte/mesoporous silica
Ionic transportation
Photoresponsive

ABSTRACT

We present a comprehensive research on the photo-induced multi-responsibility of azobenzene(azo) diblock copolymer (BPC) grafted from the surface of mesoporous silica as a light-triggered and controllable ions transport system. The surface-initiated RAFT method was used to grow sequentially a first poly(2-(dimethylamino)ethyl methacrylate) (PDMAEMA) block serving as an inner layer for the pH and thermal responsibility and a second terminal azo block functionalizing the *trans-cis* photoisomerization to control the closure or opening of the brushes in water. We show that the ions conductivity of hybrid system could be controlled by the second block switchable between the coil-recoil brush chain states in response to pH or temperature change or exposure to light. It was confirmed a suitable composition ratio of azo BPC brushes could significantly influence the hydrophilicity and polarity of the out layer with light, resulting the protonation or gelation of PDMAEMA block. For example, the $Ru(NH_3)_6^{3+}$ cations as probing ions was employed to prototyping the controlled permselectivity triggered by the UV light exposure. This kind of hybrid material is particularly interesting in the versatile utility for drug delivery, separating, biomimic sensor and so on.

1. Introduction

Over the past decade, nanoporous materials are attracting progressive interests for their significance in science, including separation [1–3], sensing [4,5], catalysis [6,7], and novel medical devices [8–11]. Especially, design biotic analogues of ion transportation through nanochannels are flourishing due to their prominent applications in smart sensors, gated switches, and commutation of the chemical species in aqueous environment [12–15]. So far, most of these applications are based on gating the nanochannel flux by nonconvalent interactions of surface-immobilized moieties with the diffusing species or by using responsive polymer brushes

* Corresponding authors at: National Engineering Research Center of Novel Equipment for Polymer Processing, The Key Laboratory of Polymer Processing Engineering of Ministry of Education, South China University of Technology (T. Kuang). Department of Mechanical Engineering, Northwestern University (L. Chang). College of Materials Science and Engineering, Zhejiang University of Technology, Hangzhou 310014, China (F. Chen).
E-mail addresses: ktrmonarch0914@gmail.com (T. Kuang), lingqian.chang@northwestern.edu (L. Chang), jacksonchen008@163.com (F. Chen).
[1] These authors contributed equally to this work.

http://dx.doi.org/10.1016/j.cej.2017.04.048
1385-8947/

that can "open" and "close" the pores [16–18], which depends on the change of physicochemical environment across the channel.

Inorganic nanoporous materials, such mesoporous silica [19], zeolite [20] and anode alumina [21] are attractive candidates for controlling nanochannel flux and ion transportation, owing to their intrinsic porosity, uniform pore size, high surface area, and permeability, which render highly-active surface and adsorption kinetic. Mesoporous silica has been considered as precise control of drug delivery [22–28] and highly-effective catalysts [29,30]. The next challenge has focused on promoting external-stimuli responsibility [31], including pH [32–35], temperature [36,37], magnetic/electronic field [38,39], chemical source[40], and specific light wave [41,42]. Herein, photoresponsive materials are particularly attractive for remote and accurate controlling in spatial and temporal conditions [43].

Azobenzene is one of the most widely utilized chromophores for producing photoresponsive materials. It can be reversibly transformed between the *trans* and *cis* isomers upon UV–*vis* light irradiation, exhibiting precise chemical changes in size and polarity [44,45]. Isomerization of azobenzene-containing (referred as azo hereafter) materials brings on photochemical pK_a changes, which might cause changes in absorption [46,47], hydrogen bond strength [48,49], and self-assembling for "smart" molecular machine [50,51] and artificial muscle [52,53]. To date, azo polymers and block copolymers (BCPs) represent two active research fields. The former one is the research highlight for exploring photoresponsive polymers [54]. The latter one is much attractive for the microphase separation and related self-organized morphology both in solid and in solution [55–57]. Recently, various azo BCPs have been promoted by the facilitation of controlled radical polymerization such as controlled radical polymerizations such as atom transfer radical polymerization (ATRP) [58] and reversible addition–fragmentation chain transfer polymerization (RAFT) [59]. Of particular interest is the remote switcher of "smart" molecular machine. This often needs ingenious design of azo BCPs. For instance, high efficiency of multi-drug release can be achieved by dual-responsive azo BCPs [60,61]. And the cloud point temperature of thermo-responsive polymers can be greatly shifted by azo blocks [62]. For the application of ion transportation, in recent years, azo compounds have been applied in the fabrication of mesoporous silica hybrid [63–66], combining photoresponse and self-assembling of variable molecules for switchable nanopores [67,68]. It is desirable for introducing azo BCPs to switch nanopore size and promote multi-stimuli responses.

Previously, we have reported on dual-responsive polyelectrolyte/mesoporous silica hybrid materials based on the self-organization of poly(2-(dimethylamino)ethyl methacrylate) (PDMAEMA) with reversible on/off responses to pH and temperature [69]. The ionized nanopore interior of this hybrid material enabled to selectively transport the counter-ion. And the gelation of PDMAEMA above lower critical solution temperature (LCST) was able to switch the nanopore size and further prompt the ion permeability. We now report on photoresponsive PDMAEMA/mesoporous silica hybrid materials by incorporating azo BCPs, which was synthesized by a surface-initiated RAFT method. Notably, upon the UV-light exposure the coil/recoil response of PDMAEMA increased as a result of *trans-cis* isomerization. The polarity and self-organization of azo BCPs were remotely controlled, leading photoresponsive ion transportation.

2. Experimental

2.1. Materials

Acrylamido azobenzene (modified azo, referred to MAzo), 2,2-azobisisobutyronitrile (AIBN), Dimethylacetamide (DMAc), *N*,*N*-dimethyl aminoethyl methacrylate (DMAEMA), methanol and absolute ethanol were purchased from Aladdin Chemistry Co. Ltd, China. Mesoporous silica (SBA-15), which had an average diameter of 8 nm, was purchased from XFNANO Materials Tech Co. Ltd, China.

2.2. Preparation of P(DMAEMA-b-PMAzo)/SBA-15 hybrids

The synthesis of amine-functionalized SBA-15 and PDMAEMA/SBA-15 precursor were based on method of our previous work [69]. P(DMAEMA-*b*-MAzo)$_{100}$/SBA-15 hybrid was synthesized by reversible addition-fragmentation chain transfer (RAFT) polymerization using MAzo as a functional monomer. For example, MAzo (5 mol% ratio) and PDMAEMA/SBA-15 precursor (95 mol% ratio) were completely dissolved in DMAc solvent. After ultrasonic dispersing for 30 min, AIBN (initiator) was added to the mixture, followed by vigorous stirring at 70 °C with oil bath for 24 h and then degassing with nitrogen for 1 h at room temperature. The reaction was stopped by quenching in ice water, and then the obtained product was washed more than 5 times with methanol to remove the residue. Finally, the purified P(DMAEMA$_{95}$-*b*-MAzo$_5$)$_{100}$/SBA-15 was dried at 60 °C for 12 h and kept for further use.

2.3. Characterization

Fourier transform infrared spectroscopy (FTIR) measurements were carried out using a Nicolet 6700 spectrometer (USA). The samples were analyzed in absorbance mode in the range of 400 to 4000 cm^{-1} with a resolution of 4 cm^{-1}. Thermogravimetric analysis (TGA) was investigated using a thermogravimetric analyzer (SDTQ600, USA). All samples were heated from room temperature to 800 °C at a heating speed of 10 °C/min under nitrogen atmosphere. Transmission electron microscopy (TEM) was performed on a CM 200FEG transmission electron microscope operated at 200 keV. The N_2 adsorption-desorption isotherms were measured on a Micromeritics ASAP 2020C+ system (USA). The total surface area, pore size distributions and pore volume were determined by BET and BJH (Barrett-Joyner-Halenda) equations based on the adsorption data. ^{1}H NMR spectra and gel permeation chromatography (GPC) were measured on a Bruker Avance III (Switzerland) and Waters 1525 (USA) with tetrahydrofuran as a mobile phase using polystyrene (PS) samples as standard tabs, respectively. The hybrids were dissolved in diluted hydrofluoride acid (HF, 1 wt%) to obtain pure BCPs for the characterization. UV–vis-NIR spectrum was conducted on a Perkin Elmer spectrophotometer (Lambda 750, USA) with a wavelength of 250–500 nm. The electrochemical experiment was performed in a three-electrode cell system. Electrochemical impedance spectroscopy (EIS) experiments and Cyclic Voltammetry (CV) were performed in 0.1 M KCl aqueous solution with 5.0 mM $Fe(CN)_6^{4-/3-}$ as the probe using RST4800 (Suzhou RST Co. China) electrochemical work station.

3. Results and discussion

3.1. Fabrication of P(DMAEMA-b-MAzo)$_{100}$/SBA-15 hybrids

Photosensitive azo BCPs were prepared by a "grafting-from" polymerization strategy (Fig. 1), in which amino groups of APTES were anchored on the porous surface of SBA-15, consecutively following the condensation of the carboxyl groups of DDMAT, the leaving groups of the RAFT agent. Afterwards serious BCP brushes of P(DMAEMA-*b*-MAzo) were synthesized d by a two-step RAFT polymerization with PDMAEMA as the first-stage monomer. The degree of polymerization (DP) was designed as 100 for the sake of suitable nanopore size and grafting amount of the as-prepared

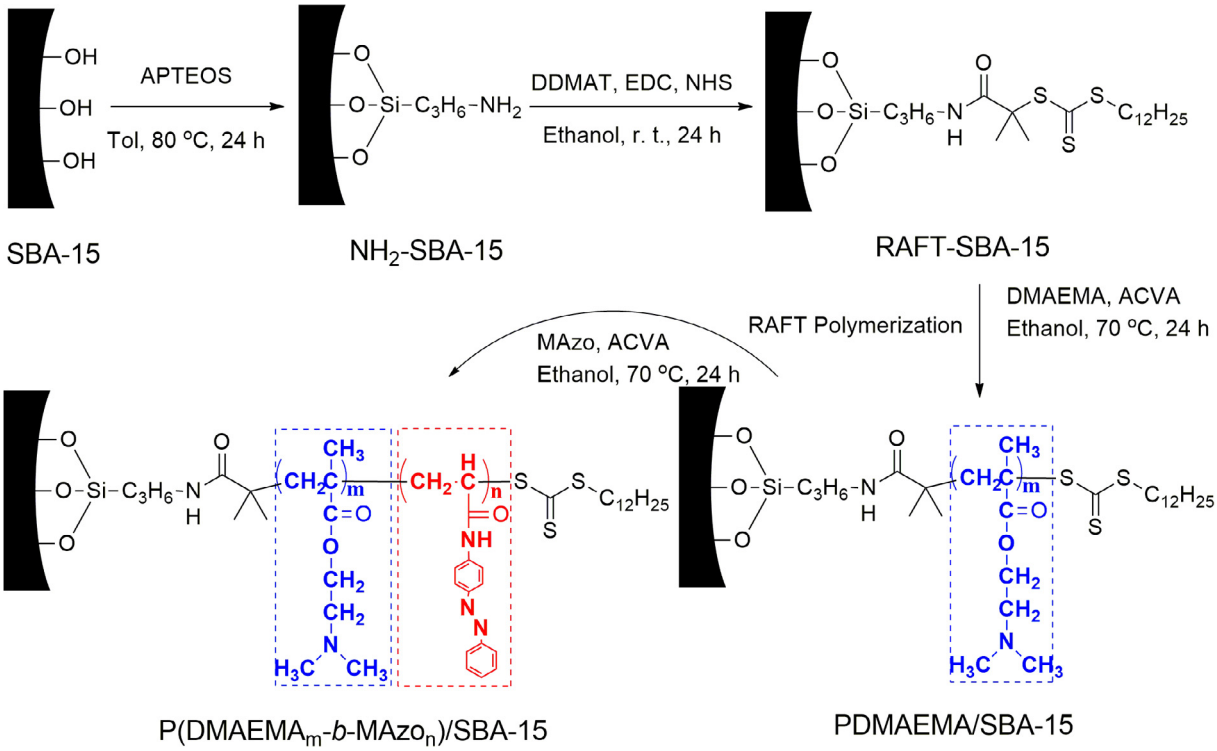

Fig. 1. The synthesis protocol of P(DMAEMA-*b*-MAzo)/SBA-15 hybrid materials.

hybrid materials [69]. The content of MAzo segments was varied from 1 to 20 mol%. FTIR confirmed the modification of the surface of SBA-15, the grafting of RAFT agent and P(DMAEMA$_{80}$-*b*-MAzo$_{20}$)$_{100}$ (Fig. 2a). A represented C=O vibration was found at 1730 cm^{-1}, confirming that the successful grafting of PDMAEMA brushes. Following the block copolymerization of the MAzo monomers, the characteristic vibrations of PMAzo segments were assigned at 1450 cm^{-1} for a new N=N vibration and 3280 cm^{-1} for a —NH— vibration. The grafting loading of P(DMAEMA-*b*-MAzo)$_{100}$ was calculated by the TGA method. Fig. 2b shows a weight loss of the hybrid material raised between 200 and 500 °C due to the surface grafting of polymer brushes. In comparison of modified SBA-15 before the polymerization, the grafting amount of P(DMAEMA$_{80}$-*b*-MAzo$_{20}$)$_{100}$ can be calculated around 19.5 wt%. The TEM image (Fig. 2c) shows a uniform contract of aligned nanochannel structure on the hybrid materials with 3 nm in width as compared the original width of original SBA-15 (Fig. S1). The polymer brushes successfully grafted to the inner surface of SBA-15 mesoporous nanoparticles, indicating that the polymerization of DMAEMA and MAzo monomers didn't destroy the mesoporous structure of SBA-15. To some extent, the exterior surface of SBA was obviously coarser (Fig. 2d).

N_2 adsorption/desorption isotherms with the corresponding pore-size distribution of the hybrid material are shown in Fig. 3a. Nitrogen adsorption/desorption isotherms for all samples show type IV pattern according to the IUPAC classification, with well-defined capillary condensation step and exhibit obvious H1 hysteresis loops in the partial pressure range of 0.4–0.8, which are attributed to the presence of mesopores in the obtained functionalized SBA-15. Structural properties of the various mesoporous samples, calculated from the adsorption/desorption isotherm by using the Barrett-Joyner-Halenda (BJH) method, are summarized in Table 1. All samples show good uniformity, with narrow pore size distribution around 3.5 nm (Fig. 3b). The decreases in the pore size values, surface area and pore volume also demonstrate the successful immobilization of polymer brushes in the mesopores channel of the SBA-15.

GPC analysis of functionalized SBA-15 products with different comonomer ratio is shown in Fig. 3c and the analysis result for all materials is summarized in Table 2. As shown in Fig. 3c and Table 2, the copolymers of various P(DMAEMA-*b*-MAzo)$_{100}$ have the similar molecular weights with theory MAzo/DMAEMA = 1/99, 5/95, 10/90 and 20/80. Meanwhile, copolymers have narrow molecular weight distributions (polydispersity, PDI) in a range of 1.16–1.21, which follow the unique law of RAFT polymerization. The block segment can be confirmed by ^{1}H NMR spectrum (Fig. 3d) and calculated from the integral areas of specific signals of PDMAEMA and PMAzo segments. Compared with the feed ratios of comonomers, the experimental copolymers have near-theory block structures (Table 2). Furthermore, TGA analysis was conducted to quantitate the grafting amount of block copolymer (Fig. 2b). After the surface-initiated RAFT reaction, the functionalized SBA-15 hybrids consisted of around 10 wt% P(DMAEMA-*b*-MAzo)$_{100}$ brushes (Table 2). The grafted copolymer brushes denote significant environmental responsibility in various conditions.

3.2. UV–Vis transformation of P(DMAEMA-b-MAzo)$_{100}$/SBA-15 hybrids

The photoresponsive properties of the P(DMAEMA-*b*-MAzo)$_{100}$/SBA-15 hybrids were investigated by various techniques. UV light in a range of 320–400 nm was used to trigger the *trans-cis* isomerization of azo groups. In this study, all hybrid materials showed significant phenomenon of the *trans-cis* isomerization. For instance, Fig. 4a shows UV–vis spectra of P(DMAEMA$_{95}$-*b*-MAzo$_5$)$_{100}$/SBA-15 hybrid with increasing UV light irradiation time (up to 15 min) and revealed a large decrease of *trans* conformation (π-π^*), which was assigned as a strong wavelength at 365 nm. Besides, the *cis* conformation (n-π^*) absorbed around 440 nm was increased. These are typical observations for the isomerization of azo groups [46]. The *cis-trans* isomerization can occur by ther-

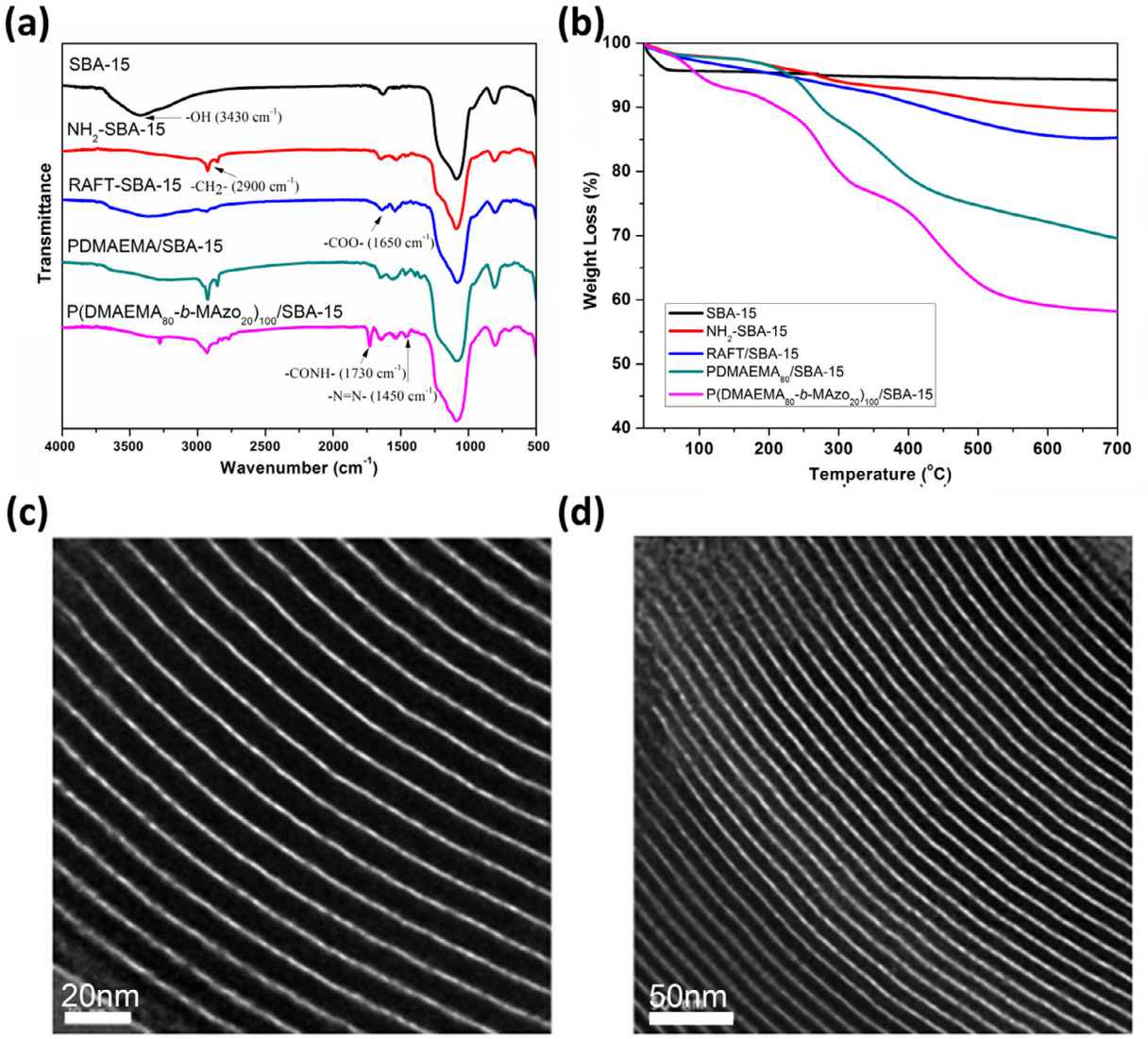

Fig. 2. The representative (a) FTIR spectra and (b) TGA curves of P(DMAEMA$_{80}$-*b*-MAzo$_{20}$)$_{100}$/SBA-15 hybrid derived by the surface-initiated RAFT polymerization method and (c and d) its TEM images.

mal relaxation and exposure to visible light. White light irradiation at room temperature revealed an excellent response (Fig. 4b). After 15 min the hybrid reached a photostationary state, while the absorbance didn't reach the same value as the pristine hybrid. This phenomenon is similar to the *cis-trans* isomerization of pristine MAzo monomer [46]. The hybrid was also allowed to relax back at higher temperature in the dark (Fig. S2). However this process took as slow as several hours. This allows us to investigate the UV-exposed hybrids with other techniques without large changes in the *trans-cis* ratio in the material.

We attempted to directly observe the photochange in the pore size by the measurement of N_2 adsorption/desorption isotherms. As azo structure transforms from *trans* to *cis* conformation, the molecular size decreases from 9.0 to 5.6 Å. The *trans* isomer has no dipole moment, while the nonplanar *cis* isomer has a dipole moment of 3.0 D. For cases of low azo-containing samples, as summarized in Table 1, no changes in pore size were observed. This result is similar to others' reports [46]. This is probably due to the adsorption of N_2 molecules on the free space between the surface azo groups. In case of P(DMAEMA$_{80}$-*b*-MAzo$_{20}$)$_{100}$ grafted hybrid, a change of 1.1 nm in the pore size was the evidence that the *trans-cis* isomerization occurred after the UV light irradiation. Besides, it was expected that the flexible PDMAEMA segment might also contribute the fast response of block copolymer upon light stimuli and promote the *trans-cis* isomerization. Furthermore, because the PDMAEMA segments possess both pH and thermal responsibilities, the as-synthesized hybrids exhibit three responding switches. Considering the ideal diblock structure of P(DMAEMA-*b*-MAzo)$_{100}$ brushes, various simultaneous responses can be created, witch can meet multiple requirement in sensory engineering.

3.3. Multi-stimuli controlled ions permeability

The fabrication of P(DMAEMA-*b*-MAzo)$_{100}$/SBA-15 hybrids sensors was performed following the spin-coating procedure on carbon electrodes [69]. In these cases, the thickness of the nanoporous hybrids films were adjusted in the range of 2–5 μm and the uniformity of as-prepared films was also controlled, as reported in Fig. S3. The sensor was characterized using electrochemical impedance spectroscopy (EIS) in a 100 mM KCl solution with a three-electrode cell system to obtain the mesoporous film's bulk resistance (R_b), which could be used to calculate the ionic conductivity through the mesoporous channels.

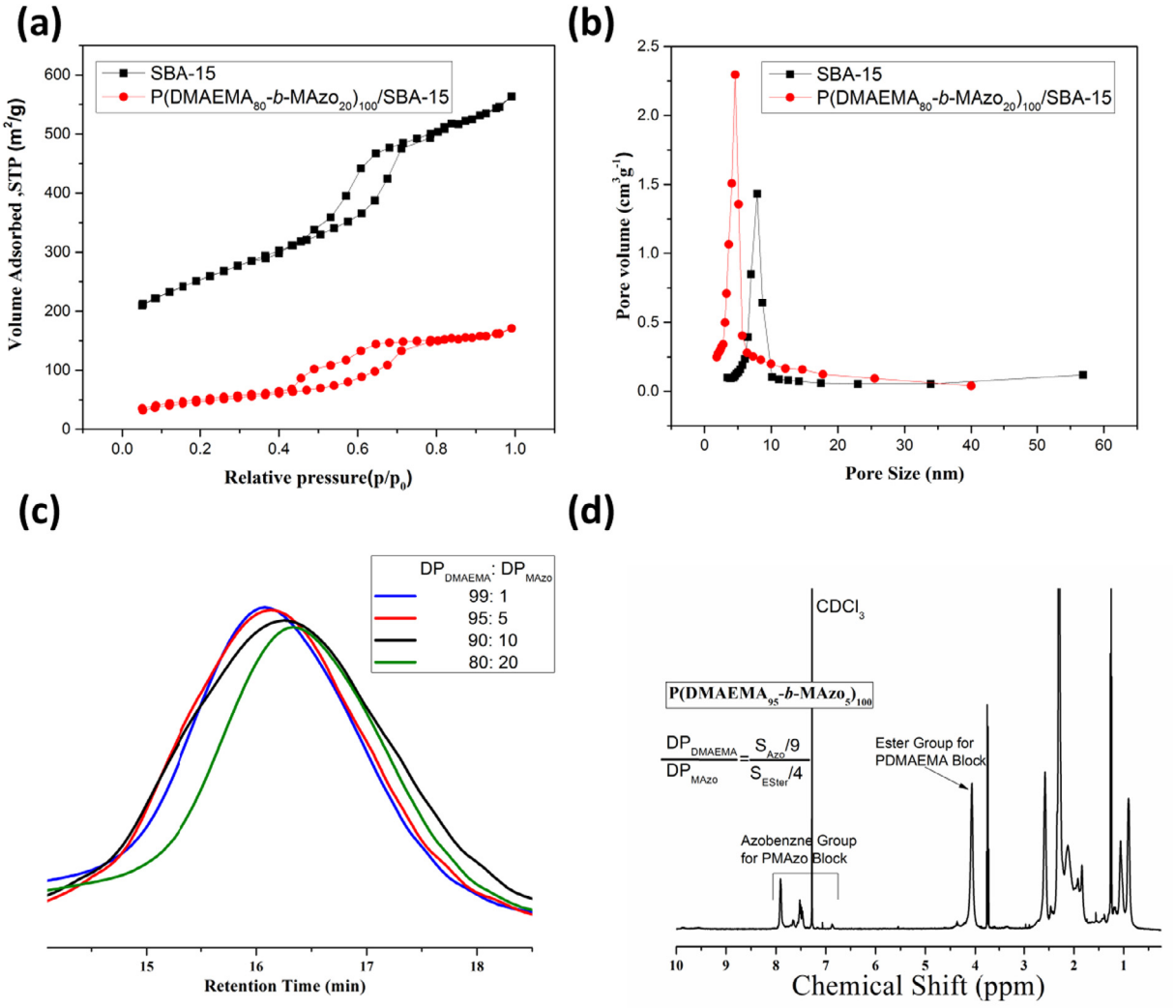

Fig. 3. The representative (a) N_2 absorption/desorption isotherm and pore size distribution of P(DMAEMA$_{80}$-*b*-MAzo$_{20}$)$_{100}$/SBA-15 hybrid. (c) The GPC curves of various BCPs separated from different hybrid materials. (d) The representative ^{1}H NMR curve of P(DMAEMA$_{95}$-*b*-MAzo$_5$)$_{100}$ BCP.

Table 1
Characterizations of mesoporous silica and its hybrid materials under visible and UV light exposure.

DP_{DMAEMA}:DP_{MAzo}	Pore Size[a] (nm)		S_{BET}[b] ($m^2\ g^{-1}$)		Pore Volume[a] ($cm^3\ g^{-1}$)	
	Vis[c]	UV[d]	Vis[c]	UV[d]	Vis[c]	UV[d]
SBA-15	7.9	7.9	513	513	0.87	0.87
99:1	3.90	3.85	127.21	121.34	0.25	0.25
99:5	4.09	3.99	132.72	132.41	0.22	0.21
90:10	4.01	3.98	132.19	135.25	0.23	0.23
80:20	3.44	4.60	128.61	136.37	0.22	0.22

[a] The average pore size and pore volume were calculated by BJH method.
[b] The specific surface area was calculated by BET method.
[c] The *trans*-conformation of azo groups was kept under the visible light.
[d] The *cis*-conformation of azo groups was transmitted under the UV light for 30 min and was tested in dark.

Table 2
Characterizations of various BCP brush structures.

BCP Brush Structure	DP_{DMAEMA}:DP_{MAzo}		M_n[b]		M_w/M_n[b](PDI)	Grafting Amount[c]
	Theory	^{1}H NMR[a]	Theory	GPC		
P(DMAEMA$_{99}$-*b*-MAzo$_1$)$_{100}$	99:1	94:1	15,793	14,940	1.15	14.7%
P(DMAEMA$_{95}$-*b*-MAzo$_5$)$_{100}$	95:5	89:4	16,165	14,970	1.19	15.4%
P(DMAEMA$_{90}$-*b*-MAzo$_{10}$)$_{100}$	90:10	83:8	16,630	15,030	1.21	17.6%
P(DMAEMA$_{80}$-*b*-MAzo$_{20}$)$_{100}$	80:20	74:17	17,560	15,800	1.20	19.5%

[a] The segment ratios of various BCP brushes were characterized by ^{1}H NMR method in $CDCl_3$ solution and calculated on the integrated area ratios between —CO—O—CH_2— group of PDMAEMA block and benzene groups of PMAzo block.
[b] The molecular weights and their polydispersities were characterized by GPC method.
[c] The grafting amounts of various BCP brushes were calculated by TGA method.

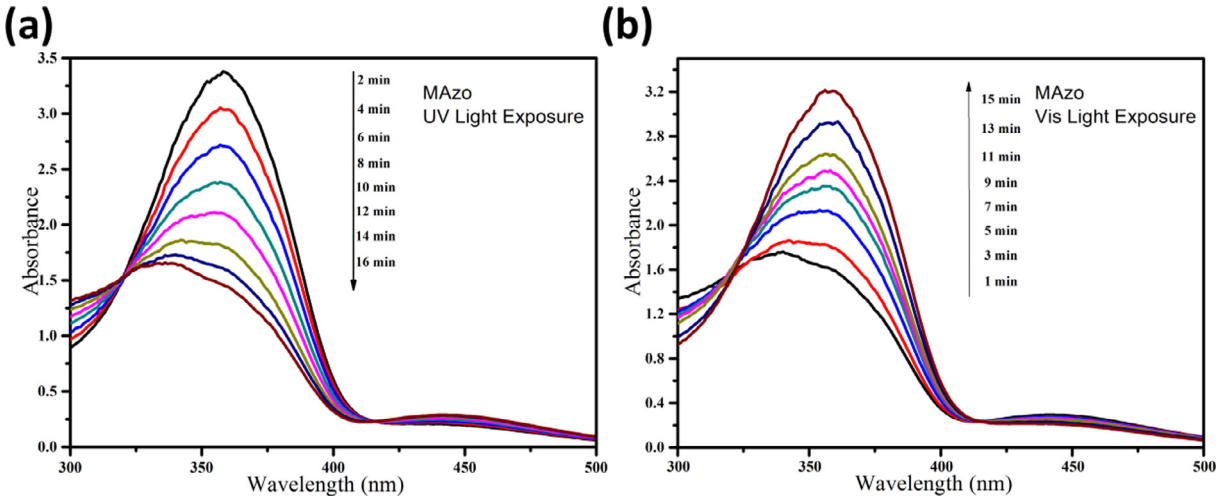

Fig. 4. The representative UV–vis spectra of P(DMAEMA$_{95}$-*b*-MAzo$_5$)$_{100}$/SBA-15 hybrid, including (a) the *trans-cis* isomerization under UV light exposure and (b) the *cis-trans* isomerization under vis light exposure.

The pH and thermal dual-responsive characters of PDMAEMA segments allowed the variation of hydrodynamic radius in response to changes in the pH or temperature in aqueous medium. However, the hydrophobic and dense blocks containing *trans*-azo groups may preclude the responsibility of PDMAEMA brushes, due to the poor solubility in water and zero dipole of *trans*-azo groups. In order to confirm this, we incubated the hybrid sensors in aqueous medium with different pH values from 4 to 10. Repre-

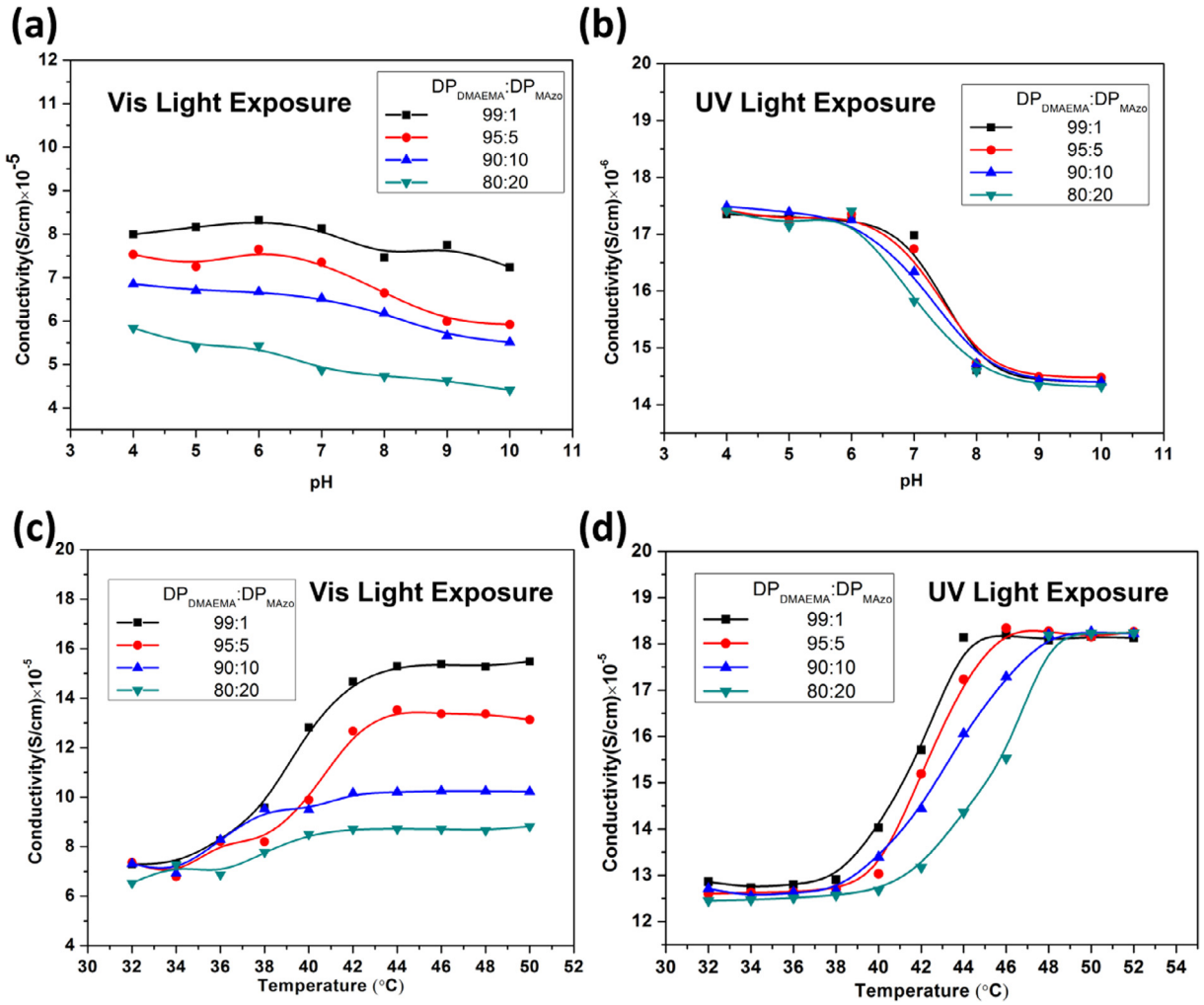

Fig. 5. The ionic conductivity of different hybrid materials as a function of pH at room temperature (a) under vis light exposure and (b) under UV light exposure. The ionic conductivity as a function of temperature at pH 10 (c) under vis light exposure and (d) under UV light exposure.

sentative ion conductivities of the product sensors following different pH and light treatments are provided in Fig. 5. Incubation in basic water under visible light caused vary weak changes in ion conductivity. In comparison, after UV light irradiation, the sensors exhibited significantly sensibility and ionic conductivities alter rapidly between 7 and 8, which in accord with previous reported (PDMAEMA p*K*a = 7.4) [70–72]. In this state, the *cis* conformation of azo groups increased the dipole and molecular spacing between azo groups, which allowed that small and polar ions could permeate the hinder of PMAzo segments and "open" the ion nanochannels, reflecting in a obvious jumping of ion conductivity. It is noteworthy that the length of PMAzo segments was effective in the change of the ion conductivity, which that high content of PMAzo segment showed much more barrier action for the ion transportation (Fig. 5a and b).

The thermo-responsibility of the product sensors further confirmed the barrier effect of *trans*-azo groups, as shown in Fig. 5c and d. It is well-known that the variation of a typical LCST behaviour on the PDMAEMA chain conformation is strongly dependent upon temperature and the corresponding pH value in aqueous medium [70,73]. Here, the LCST for a graft PDMAEMA was determined 39 °C at pH 10 [74]. In cases of the *trans* conformation, all the hybrid sensors showed the LCST at 39 °C and the change of ion conductivity was decreased with increasing molar fractions of the PMAzo segment (Fig. 5c). After the UV light irradiation, the *cis*-rich hybrid sensors showed higher LCST compared with those of *trans*-rich ones, although the large shift of the LCST only appeared at higher molar fractions of PMAzo segment as shown in Fig. 5d. This behaviour was comparable with other azo BCPs in pure water [61,69]. It is suggested that the photoisomerization exert significant effect on the intermolecular interactions between PDMAEMA and basic water, resulting a more prominent coil-globule transition characteristic of PDMAEMA in basic water [62]. These results inspired us to use the hybrid sensors to control the electrochemical switchable property triggered by UV–vis light irradiation under different solution pH or temperature.

To investigate the ionic transport properties of the hybrid interfacial assemblies, the diffusion of charged species through mesoporous films supported on electrode was electrochemically probed by CV using $Ru(CN)_6^{2+/3+}$ as a anionic redox probe. Unlike the drug-delivery cargo, this prototype probe was designed for the sensor, so the payload of transportation ions was weaken for the CV test. Before UV light irradiation, the nanopores of hybrid sensors were coated with hydrophilic PDMAEMA brushes and non-polar *trans*-azo groups at terminal. The intermolecular electrostatic action between tertiary amine groups and $Ru(CN)_6^{2+}$ cations were greatly impeded, although the PDMAEMA brushed could be of coil-globule aggregation above the LCST. In the case of $P(DMAEMA_{95}\text{-}b\text{-}MAzo_5)_{100}$ brushes, the conductivity of $Ru(CN)_6^{2+}$ cations was almost the same with respect to the change of temperature (Fig. 6a). After the UV light irradiation, the polar *cis*-azo groups were no longer the barriers to the diffusion and electrostatic interaction of $Ru(CN)_6^{2+}$ cations, reflecting in assignable electrochemical response of $Ru(NH_3)_6^{3+}$ cations (Fig. 6b). As expected, further increasing temperature above LCST (40 °C) evidenced a more pronounced gating response of the interfacial assembly because PDMAEMA brushes were fully deprotonated, and the freely mobile expanded chains collapse inside the pores.

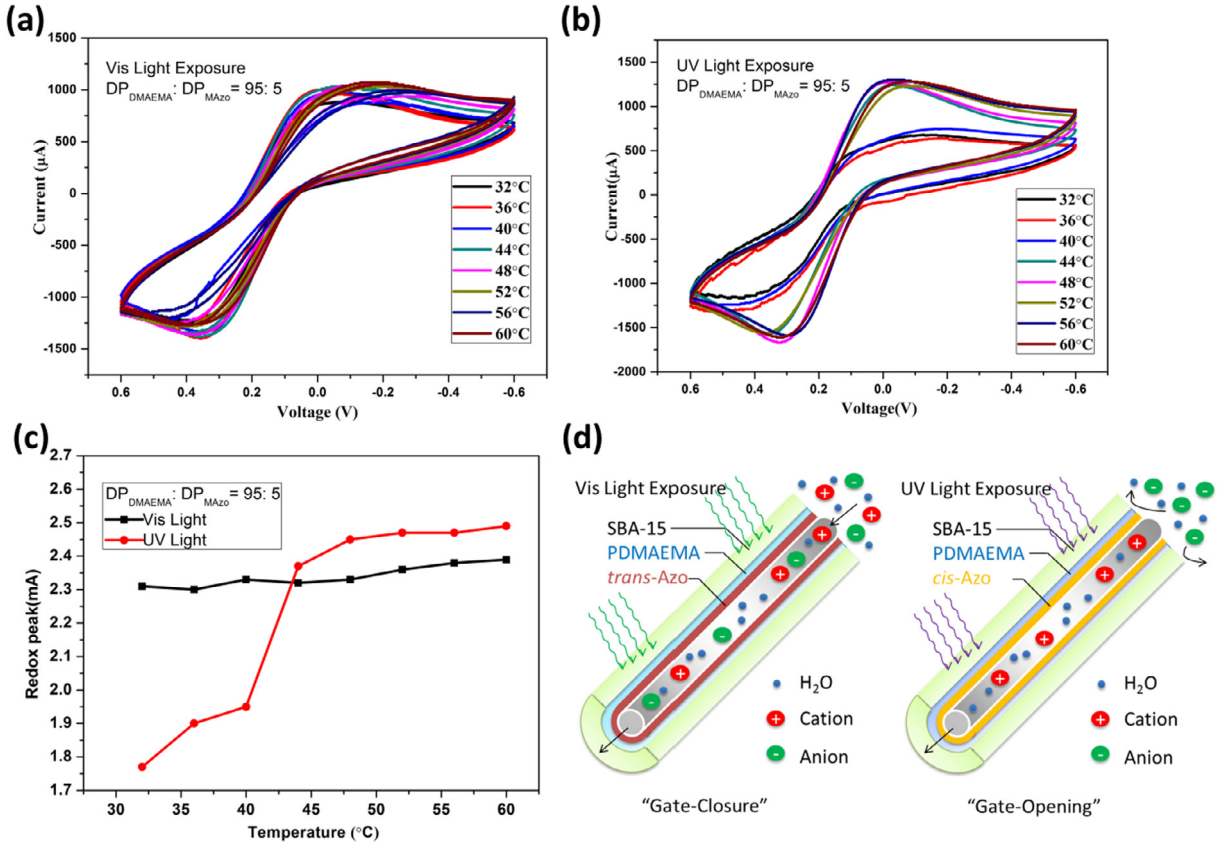

Fig. 6. Comparative cyclic voltammograms displaying the molecular transport through P(DMAEMA95-b-MAzo5)100/SBA-15 mesoporous films as functions of temperature at pH = 10 and using Ru(NH3)62+/3+ as a cationic redox probe, (a) under vis light exposure and (b) under UV light exposure. (c) The redox peak current of as-prepared device as functions of temperature. Electrolyte: 1 mM redox probe + 100 mM KCl. (d) The possible mechanism of the "gate-on/off" effect of P(DMAEMA-b-MAzo)100/SBA-15 hybrid materials, switched by UV/vis light exposure.

Fig. 6c compared the peak values of electrochemical response of Ru$(NH_3)_6^{3+}$ cations trigger by UV light irradiation, illustrating excellent gate-control for permslective transport of cations. Furthermore, the LCST of P(DMAEMA-*b*-MAzo) BCPs can be adjusted by modifying the MAzo ratio. For example, P(DMAEMA$_{80}$-*b*-MAzo$_{20}$)$_{100}$ brushes exhibited higher LCST (44 °C) and the as-prepared sensor showed a more enhancive change of electrochemical response of Ru$(NH_3)_6^{3+}$ cations as shown in Fig. S4. Delighted by aforementioned results, we proposed the terminal segment containing azo groups was essential to implement the environmental response of PDMAEMA brushes. The *trans* conformation of azo groups could greatly preclude the intermolecular interactions and transportation of ions. When the UV light excited the isomerization of azo groups, the *cis* conformation showed larger polarity and smaller molecular size, inducing significant pH/thermal-responsibility of PDMAEMA brushes as schemed in Fig. 6d.

4. Conclusions

We have modified the nanopores of SBA-15 with pH and thermal dual-responsive PDMAEMA BCPs that the terminal segment contains a number of azo group, employing surface-initiated RAFT polymerization from the inner wall of nanopores. The hybrid structures exhibit well-defined diblock and homogeneous covering of the polymer brushes, forming a biomimetic smart ionic channel with high potential for various environmental stimuli. Being grafted from the inner wall of nanopores, while the terminal azo-containing block can be either non-polar and dense (*trans* conformation) or polar and loose (*cis* conformation) triggered by UV–vis light exposure, the water solubility of the inner layer (PDMAEMA) can be switched in response to pH or temperature change. We found that upon the increase of azo groups, change of ion transportation was greatly effect by the photoisomerization of azo groups. After the UV light exposure, when the *cis*-azo content is above 5%, PDMAEMA chains become essentially deprotonized at pH >7.4 and gelated at T > LCST, undergoing coil-recoil transition likes PDMAEMA in water alone. On the other side, under the visible light irradiation, the *trans*-azo segments have poor solubility in water and non-polarity for hydrone and ions, resulting that there is little coil-recoil transition of PDMAEMA chains. And a much large photoinduced LCST shift as a result of *trans-cis* isomerization of azo group was observed. In light of the results, a prototype of light-triggered hybrid sensor was fabricated. The cationic probe can be permeated at high pH and T > LCST under UV light irradiation, presenting a "gate-on" state. The non-selectivity can be quickly switched by exposing the visible light, presenting a "gate-off" state. Because of the environment selective conformational behaviour, the as-designed system can give the potential for being a versatile multi-stimuli-responsive nanodevice.

Acknowledgements

The authors acknowledge the financial support of National Natural Science Foundation of China (NO. 51303158 and 51673175), and the Natural Science Foundation of Zhejiang Province (NO. LY15E030005 and LY17E030006).

Appendix A. Supplementary data

Supplementary data associated with this article can be found, in the online version, at http://dx.doi.org/10.1016/j.cej.2017.04.048.

References

[1] M.B. Shiflett, H.C. Foley, Ultrasonic deposition of high-selectivity nanoporous carbon membranes, Science 285 (1999) 1902–1905.
[2] H.W. Kim, H.W. Yoon, S.M. Yoon, B.M. Yoo, B.K. Ahn, Y.H. Cho, H.J. Shin, H. Yang, U. Paik, S. Kwon, J.Y. Choi, H.B. Park, Selective gas transport through few-layered graphene and graphene oxide membranes, Science 342 (2013) 91–95.
[3] J. Liu, N.P. Wickramaratne, S.Z. Qiao, M. Jaroniec, Molecular-based design and emerging applications of nanoporous carbon spheres, Nat. Mater. 14 (2015) 763–774.
[4] X. Zhao, X.H. Bu, T. Wu, S.T. Zheng, L. Wang, P.Y. Feng, Selective anion exchange with nanogated isoreticular positive metal-organic frameworks, Nat. Commun. 4 (2013) 2344.
[5] T. Kuang, L. Chang, X. Peng, X. Hu, D. Gallego-Perez, Molecular beacon nanosensors for probing living cancer cells, Trends Biotechnol. 35 (2017) 347–359.
[6] T.W. Kim, K.S. Choi, Nanoporous BiVO4 photoanodes with dual-layer oxygen evolution catalysts for solar water splitting, Science 343 (2014) 990–994.
[7] J.T. Zhang, C.M. Li, Nanoporous metals: fabrication strategies and advanced electrochemical applications in catalysis, sensing and energy systems, Chem. Soc. Rev. 41 (2012) 7016–7031.
[8] L. Chang, L. Li, J. Shi, Y. Sheng, W. Lu, D. Gallego-Perez, L.J. Lee, Micro-/nanoscale electroporation, Lab Chip 16 (2016) 4047–4062.
[9] Q.L. Li, Y.F. Sun, Y.L. Sun, J.J. Wen, Y. Zhou, Q.M. Bing, L.D. Isaacs, Y.H. Jin, H. Gao, Y.W. Yang, Mesoporous silica nanoparticles coated by layer-by-layer self-assembly using cucurbit[7]uril for in vitro and in vivo anticancer drug release, Chem. Mater. 26 (2014) 6418–6431.
[10] L. Chang, J. Hu, F. Chen, J. Shi, Z. Yang, Y. Li, L.J. Lee, Nanoscale bio-platforms for living cell interrogation: current status and future perspectives, Nanoscale 8 (2016) 3138–3206.
[11] E. Tasciotti, X.W. Liu, R. Bhavane, K. Plant, A.D. Leonard, B.K. Price, M.M.C. Cheng, P. Decuzzi, J.M. Tour, F. Robertson, M. Ferrari, Mesoporous silicon particles as a multistage delivery system for imaging and therapeutic applications, Nat. Nanotechnol. 3 (2008) 151–157.
[12] C. Dekker, Solid-state nanopores, Nat. Nanotechnol. 2 (2007) 209–215.
[13] X. Hou, W. Guo, L. Jiang, Biomimetic smart nanopores and nanochannels, Chem. Soc. Rev. 40 (2011) 2385–2401.
[14] W. Guo, Y. Tian, L. Jiang, Asymmetric ion transport through ion-channel-mimetic solid-state nanopores, Acc. Chem. Res. 46 (2013) 2834–2846.
[15] L.Q. Chang, D. Gallego-Perez, C.L. Chiang, P. Bertani, T.R. Kuang, Y. Sheng, F. Chen, Z. Chen, J.F. Shi, H. Yang, X.M. Huang, V. Malkoc, W. Lu, L.J. Lee, Controllable large-scale transfection of primary mammalian cardiomyocytes on a nanochannel array platform, Small 12 (2016) 5971–5980.
[16] H.C. Zhang, Y. Tian, L. Jiang, Fundamental studies and practical applications of bio-inspired smart solid-state nanopores and nanochannels, Nano Today 11 (2016) 61–81.
[17] S.F. Buchsbaum, G. Nguyen, S. Howorka, Z.S. Siwy, DNA-modified polymer pores allow pH- and voltage-gated control of channel flux, J. Am. Chem. Soc. 136 (2014) 9902–9905.
[18] H.C. Zhang, Y. Tian, J. Hou, X. Hou, G.L. Hou, R.W. Ou, H.T. Wang, L. Jiang, Bioinspired smart gate-location-controllable single nanochannels: experiment and theoretical simulation, ACS Nano 9 (2015) 12264–12273.
[19] X.Y. Lin, Q. Yang, L.H. Ding, B. Su, Ultrathin silica membranes with highly ordered and perpendicular nanochannels for precise and fast molecular separation, ACS Nano 9 (2015) 11266–11277.
[20] B. Said, A. Grandjean, Y. Barre, F. Tancret, F. Fajula, A. Galarneau, LTA zeolite monoliths with hierarchical trimodal porosity as highly efficient microreactors for strontium capture in continuous flow, Microporous Mesoporous Mater. 232 (2016) 39–52.
[21] S.M. Wu, F. Wildhaber, O. Vazquez-Mena, A. Bertsch, J. Brugger, P. Renaud, Facile fabrication of nanofluidic diode membranes using anodic aluminium oxide, Nanoscale 4 (2012) 5718–5723.
[22] T.R. Kuang, Y.R. Liu, T.T. Gong, X.F. Peng, X.L. Hu, Z.Q. Yu, Enzyme-responsive nanoparticles for anticancer drug delivery, Curr. Nanosci. 12 (2016) 38–46.
[23] Y.W. Yang, Towards biocompatible nanovalves based on mesoporous silica nanoparticles, MedChemComm 2 (2011) 1033–1049.
[24] Z.L. Wu, N. Song, R. Menz, B. Pingali, Y.W. Yang, Y.B. Zheng, Nanoparticles functionalized with supramolecular host-guest systems for nanomedicine and healthcare, Nanomedicine 10 (2015) 1493–1514.
[25] K. Patel, S. Angelos, W.R. Dichtel, A. Coskun, Y.W. Yang, J.I. Zink, J.F. Stoddart, Enzyme-responsive snap-top covered silica nanocontainers, J. Am. Chem. Soc. 130 (2008) 2382–2383.
[26] S. Angelos, Y.W. Yang, K. Patel, J.F. Stoddart, J.I. Zink, PH-responsive supramolecular nanovalves based on cucurbit[6]uril pseudorotaxanes, Angew. Chem. Int. Ed. 47 (2008) 2222–2226.
[27] S. Angelos, Y.W. Yang, N.M. Khashab, J.F. Stoddart, J.I. Zink, Dual-controlled nanoparticles exhibiting AND logic, J. Am. Chem. Soc. 131 (2009) 11344–11346.
[28] H. Zhou, X. Wang, J. Tang, Y.W. Yang, Surface immobilization of pH-responsive polymer brushes on mesoporous silica nanoparticles by enzyme mimetic catalytic ATRP for controlled cargo release, Polymers 8 (2016) 277.
[29] G.W. Zhan, H.C. Zeng, Integrated nanocatalysts with mesoporous silica/silicate and microporous MOF materials, Coord. Chem. Rev. 320 (2016) 181–192.
[30] J. Liu, L.H. Yu, Z. Zhao, Y.S. Chen, P.Y. Zhu, C. Wang, Y. Luo, C.M. Xu, A.J. Duan, G. Y. Jiang, Potassium-modified molybdenum-containing SBA-15 catalysts for highly efficient production of acetaldehyde and ethylene by the selective oxidation of ethane, J. Catal. 285 (2012) 134–144.
[31] M. Molina, M. Asadian-Birjand, J. Balach, J. Bergueiro, E. Miceli, M. Calderon, Stimuli-responsive nanogel composites and their application in nanomedicine, Chem. Soc. Rev. 44 (2015) 6161–6186.

[32] G.L. Wang, B. Zhang, J.R. Wayment, J.M. Harris, H.S. White, Electrostatic-gated transport in chemically modified glass nanopore electrodes, J. Am. Chem. Soc. 128 (2006) 7679–7686.
[33] F. Chen, X.P. Jiang, T.R. Kuang, L.Q. Chang, D.J. Fu, Z.G. Yang, J.T. Yang, P. Fan, Z. D. Fei, M.Q. Zhong, Effect of nanoporous structure and polymer brushes on the ionic conductivity of poly(methacrylic acid)/anode aluminum oxide hybrid membranes, RSC Adv. 5 (2015) 70204–70210.
[34] H. Zhou, X. Wang, J. Tang, Y.W. Yang, Tuning the growth, crosslinking, and gating effect of disulfide-containing PGMAs on the surfaces of mesoporous silica nanoparticles for redox/pH dual-controlled cargo release, Polym. Chem. 7 (2016) 2171–2179.
[35] Q.L. Li, S.H. Xu, H. Zhou, X. Wang, B.A. Dong, H. Gao, J. Tang, Y.W. Yang, PH and glutathione dual-responsive dynamic cross-linked supramolecular network on mesoporous silica nanoparticles for controlled anticancer drug release, ACS Appl. Mater. Interface 7 (2015) 28656–28664.
[36] K.Y. Chun, W. Choi, S.C. Roh, C.S. Han, Patchable, flexible heat-sensing hybrid ionic gate nanochannel modified with a wax-composite, Nanoscale 7 (2015) 12427–12434.
[37] N. Song, Y.W. Yang, Molecular and supramolecular switches on mesoporous silica nanoparticles, Chem. Soc. Rev. 44 (2015) 3474–3504.
[38] Y.H. Lin, Z.W. Chen, X.Y. Liu, Using inorganic nanomaterials to endow biocatalytic systems with unique features, Trends Biotechnol. 34 (2016) 303–315.
[39] D. Gallego-Perez, L.Q. Chang, J.F. Shi, J.Y. Ma, S.H. Kim, X. Zhao, V. Malkoc, X.M. Wang, M. Minata, K.J. Kwak, Y. Wu, G.P. Lafyatis, W. Lu, D.J. Hansford, I. Nakano, L.J. Lee, On-chip clonal analysis of glioma-stem-cell motility and therapy resistance, Nano Lett. 16 (2016) 5326–5332.
[40] B.V.V.S.P. Kumar, K.V. Rao, S. Sampath, S.J. George, M. Eswaramoorthy, Supramolecular gating of ion transport in nanochannels, Angew. Chem. Int. Ed. 53 (2014) 13073–13077.
[41] J.A. Liu, W.B. Bu, L.M. Pan, J.L. Shi, NIR-triggered anticancer drug delivery by upconverting nanoparticles with integrated azobenzene-modified mesoporous silica, Angew. Chem. Int. Ed. 52 (2013) 4375–4379.
[42] C. Hu, K.R. West, O.A. Scherman, Hollow mesoporous raspberry-like colloids with removable caps as photoresponsive nanocontainers, Nanoscale 8 (2016) 7840–7844.
[43] S. Alberti, G.J.A.A. Soler-Illia, O. Azzaroni, Gated supramolecular chemistry in hybrid mesoporous silica nanoarchitectures: controlled delivery and molecular transport in response to chemical, physical and biological stimuli, Chem. Commun. 51 (2015) 6050–6075.
[44] A. Natansohn, P. Rochon, Photoinduced motions in azo-containing polymers, Chem. Rev. 102 (2002) 4139–4175.
[45] E.W.G. Diau, A new trans-to-cis photoisomerization mechanism of azobenzene on the S-1(n, pi*) surface, J. Phys. Chem. A 108 (2004) 950–956.
[46] J. Timm, C. Stoltenberg, J. Senker, W. Bensch, Azobenzene-functionalized SBA-15 material for application in selective separation, Z. Anorg. Allg. Chem. 640 (2014) 595–603.
[47] M. Fujiwara, M. Akiyama, M. Hata, K. Shiokawa, R. Nomura, Photoinduced acceleration of the effluent rate of developing solvents in azobenzene-tethered silica gel, ACS Nano 2 (2008) 1671–1681.
[48] X. Mei, S. Yang, D.Y. Chen, N.J. Li, H. Li, Q.F. Xu, J.F. Ge, J.M. Lu, Light-triggered reversible assemblies of azobenzene-containing amphiphilic copolymer with beta-cyclodextrin-modified hollow mesoporous silica nanoparticles for controlled drug release, Chem. Commun. 48 (2012) 10010–10012.
[49] H.P.C. van Kuringen, J.W.A. Leijten, A.H. Gelebart, D.J. Mulder, G. Portale, D.J. Broer, A.P.H.J. Schenning, Photoresponsive nanoporous smectic liquid crystalline polymer networks: changing the number of binding sites and pore dimensions in polymer adsorbents by light, Macromolecules 48 (2015) 4073–4080.
[50] J.M. Abendroth, O.S. Bushuyev, P.S. Weiss, C.J. Barrett, Controlling motion at the nanoscale: rise of the molecular machines, ACS Nano 9 (2015) 7746–7768.
[51] M. Banghart, K. Borges, E. Isacoff, D. Trauner, R.H. Kramer, Light-activated ion channels for remote control of neuronal firing, Nat. Neurosci. 7 (2004) 1381–1386.
[52] S. Erbas-Cakmak, D.A. Leigh, C.T. McTernan, A.L. Nussbaumer, Artificial molecular machines, Chem. Rev. 115 (2015) 10081–10206.
[53] S. Iamsaard, S.J. Asshoff, B. Matt, T. Kudernac, J.J.L.M. Cornelissen, S.P. Fletcher, N. Katsonis, Conversion of light into macroscopic helical motion, Nat. Chem. 6 (2014) 229–235.
[54] C.J. Kang, S.N. Ramakrishna, A. Nelson, C.V.M. Cremmel, H.V. Stein, N.D. Spencer, L. Isa, E.M. Benetti, Ultrathin, freestanding, stimuli-responsive, porous membranes from polymer hydrogel-brushes, Nanoscale 7 (2015) 13017–13025.
[55] S. Wang, N. Zhang, X.P. Ge, Y.B. Wan, X.H. Li, L. Yan, Y.J. Xia, B. Song, Self-assembly of an azobenzene-containing polymer prepared by a multi-component reaction: supramolecular nanospheres with photo-induced deformation properties, Soft Matter 10 (2014) 4833–4839.
[56] X.D. Tang, X.C. Liang, L.C. Gao, X.H. Fan, Q.F. Zhou, Water-soluble triply-responsive homopolymers of N,N-dimethylaminoethyl methacrylate with a terminal azobenzene moiety, J. Polym. Sci. Polym. Chem. 48 (2010) 2564–2570.
[57] Y. Zhao, J. He, Azobenzene-containing block copolymers: the interplay of light and morphology enables new functions, Soft Matter 5 (2009) 2686–2693.
[58] S. Kumar, Y.L. Dory, M. Lepage, Y. Zhao, Surface-grafted stimuli-responsive block copolymer brushes for the thermo-, photo- and pH-sensitive release of dye molecules, Macromolecules 44 (2011) 7385–7393.
[59] N.I. Boiko, M.A. Bugakov, E.V. Chernikova, A.A. Piryazev, Y.I. Odarchenko, D.A. Ivanov, V.P. Shibaev, Liquid crystalline side-chain triblock copolymers consisting of a nematic central subblock edged by photochromic azobenzene-containing fragments: their synthesis, structure and photooptical behaviour, Polym. Chem. 6 (2015) 6358–6371.
[60] W. Xiao, X. Zeng, H. Lin, K. Han, H.Z. Jia, X.Z. Zhang, Dual stimuli-responsive multi-drug delivery system for the individually controlled release of anti-cancer drugs, Chem. Commun. 51 (2015) 1475–1478.
[61] L. Ye, X.Q. Liu, K. Ito, Z.G. Feng, The preparation of an azo-substituted polyrotaxane end-capped with PNIPPAAm and its dual stimuli-responsive behavior for drug delivery applications, J. Mater. Chem. B 2 (2014) 5746–5757.
[62] J. He, L. Tremblay, S. Lacelle, Y. Zhao, How can photoisomerization of azobenzene induce a large cloud point temperature shift of PNIPAM?, Polym Chem 5 (2014) 5403–5411
[63] A. Khabibullin, I. Zharov, Nanoporous membranes with tunable pore size by pressing/sintering silica colloidal spheres, ACS Appl. Mater. Interface 6 (2014) 7712–7718.
[64] S.F. Guo, K. Matsukawa, T. Miyata, T. Okubo, K. Kuroda, A. Shimojima, Photoinduced bending of self-assembled azobenzene siloxane hybrid, J. Am. Chem. Soc. 137 (2015) 15434–15440.
[65] D.P. Ferris, Y.L. Zhao, N.M. Khashab, H.A. Khatib, J.F. Stoddart, J.I. Zink, Light-operated mechanized nanoparticles, J. Am. Chem. Soc. 131 (2009) 1686–1688.
[66] Q.L. Li, L. Wang, X.L. Qiu, Y.L. Sun, P.X. Wang, Y. Liu, F. Li, A.D. Qi, H. Gao, Y.W. Yang, Stimuli-responsive biocompatible nanovalves based on [small beta]-cyclodextrin modified poly(glycidyl methacrylate), Polym. Chem. 5 (2014) 3389–3395.
[67] E. Aznar, M. Oroval, L. Pascual, J.R. Murguia, R. Martinez-Manez, F. Sancenon, Gated materials for on-command release of guest molecules, Chem. Rev. 116 (2016) 561–718.
[68] I. Zharov, A. Khabibullin, Surface-modified silica colloidal crystals: nanoporous films and membranes with controlled ionic and molecular transport, Acc. Chem. Res. 47 (2014) 440–449.
[69] F. Chen, X.P. Jiang, T.R. Kuang, L.Q. Chang, D.J. Fu, J.T. Yang, P. Fan, M.Q. Zhong, Polyelectrolyte/mesoporous silica hybrid materials for the high performance multiple-detection of pH value and temperature, Polym Chem 6 (2015) 3529–3536.
[70] D. Fournier, R. Hoogenboom, H.M.L. Thijs, R.M. Paulus, U.S. Schubert, Tunable pH- and temperature-sensitive copolymer libraries by reversible addition-fragmentation chain transfer copolymerizations of methacrylates, Macromolecules 40 (2007) 915–920.
[71] S. Yusa, M. Sugahara, T. Endo, Y. Morishima, Preparation and characterization of a pH-responsive nanogel based on a photo-cross-linked micelle formed from block copolymers with controlled structure, Langmuir 25 (2009) 5258–5265.
[72] W.J. Guo, T.S. Wang, X.D. Tang, Q. Zhang, F.Q. Yu, M.S. Pei, Triple stimuli-responsive amphiphilic glycopolymer, J. Polym. Sci. Polym. Chem. 52 (2014) 2131–2138.
[73] E.H. Otal, P.C. Angelome, S.A. Bilmes, G.J.A.A. Soler-Illia, Functionalized mesoporous hybrid thin films as selective membranes, Adv. Mater. 18 (2006) 934–938.
[74] F. Schacher, M. Ulbricht, A.H.E. Muller, Self-supporting, double stimuli-responsive porous membranes from polystyrene-block-poly(N,N-dimethylaminoethyl methacrylate) diblock copolymers, Adv. Funct. Mater. 19 (2009) 1040–1045.